Shock-Fitting Computational Method for the Inviscid Blunt-Body Problem

Research Project

Author: Iliya Milman
Advisor: Dr. Michael Karp
Flow Physics Lab, Faculty of Aerospace Engineering
Technion - Israel Institute of Technology
November 2023

Abstract

This study proposes an improved approach to simulate the supersonic blunt-body problem using a time-dependent shock-fitting algorithm. This new method overcomes previous challenges by utilizing boundary conditions with Riemann variables for shock acceleration and a new coordinate system which enhances the mesh at the outflow. The program provides accurate base flow for future research on the stability of flows over blunt-bodies.

1 Introduction

The blunt-body in supersonic flow is an important problem in aerodynamics because all high-speed vehicles have blunt noses to reduce aerodynamic heating. Such heating is a crucial design factor for most high-speed vehicles and its prediction requires accurate knowledge of the flow field around the body. To solve this problem numerically, a time-dependent shock-fitting algorithm is employed. The algorithm treats the shock wave as a boundary, with the flow behind the shock given analytically, using the Rankine-Hugoniot shock relations. The unsteady Euler equations are then solved until a steady state is obtained, allowing for the determination of the shock shape and the flow field between the shock and the body. This study builds upon Research Project 1 (Ref. [1]), in which the blunt-body problem was solved using the approach outlined by Anderson [2]. However, the results were unsatisfactory for several reasons, such as oscillations near the outflow boundary, limited flow field in the axisymmetric case, and sub-optimal mesh at the outflow boundary. To address these issues, a new and improved approach based on the method proposed by Salas [3] is utilized in the current work.

Notations

a	Speed of sound
p	Pressure
ρ	Density
s	Entropy
Θ	Temperature
t	Time
u	Radial velocity component
v	Angular velocity component
r	Radial coordinate
c	Shock radial coordinate
b	Body radial coordinate
θ	Angular coordinate
γ	Heat capacity ratio
f_x	subscript implies partial derivation by x

Contents

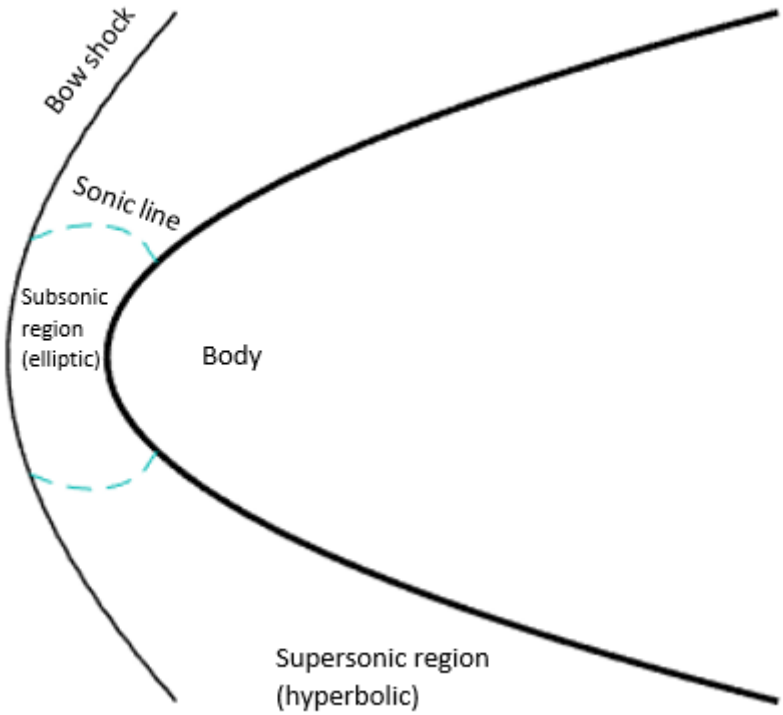

Fig. 1: The Blunt Body Problem

2 The Blunt-Body Problem

Consider the steady flow over a blunt-body moving at supersonic speed. A schematic sketch of the problem is shown in Figure 1. The shock wave in front of this body is detached and curved. The incoming flow undergoes through variable shock angles, ranging from a normal shock wave at the nose tip and approaching a weak Mach wave away from the tip. The region between the shock and the body is called the shock layer, and it contains both subsonic and supersonic flows, divided by sonic lines. Behind the normal, and nearly normal, portions of the shock wave, the flow is subsonic which is mathematically elliptic, whereas behind the more oblique portion of the shock wave the flow is supersonic which is mathematically hyperbolic.

3 The Governing Equations

In order to solve the inviscid problem, it is necessary to use the Euler equations in the appropriate form. The first step is to non-dimensionalize the equations by normalizing the flow variables with respect to their freestream values, as detailed in

appendix A. In addition, instead of using in-plane Cartesian coordinates as in our previous work [1], we switch to in-plane cylindrical coordinates to facilitate simulation of a larger portion of the outflow boundary. The governing equations, when one dimension is reduced, are written in cylindrical and spherical coordinate systems, for two-dimensional (2D) and axisymmetric flows, respectively. Since only the flow at the high-pressure side of the shock is solved, the flow is isentropic, thus, the energy equation can be replaced by an entropy convection equation. As a result of these modifications, the Euler equations take the following form

$$\begin{aligned} \rho\left(u_t + uu_r + \frac{v}{r}u_\theta - \frac{v^2}{r}\right) &= -p_r, \\ \rho\left(v_t + uv_r + \frac{v}{r}v_\theta + \frac{vu}{r}\right) &= -p_\theta, \\ \rho_t + \rho u_r + u\rho_r + \frac{\rho}{r}v_\theta + \frac{v}{r}\rho_\theta + k &= 0, \\ s_t + us_r + \frac{v}{r}s_\theta &= 0, \end{aligned} \tag{1}$$

where

$$k = \begin{cases} \frac{u}{r} & \text{cylindrical (2D)} \\ \frac{2u+v\cot\theta}{r} & \text{spherical (axisymmetric).} \end{cases} \tag{2}$$

Introducing the variable $P = \ln p$ the equations can be written as

$$\begin{aligned} u_t &= -\left(uu_r + \frac{v}{r}u_\theta - \frac{v^2}{r} + \Theta P_r\right), \\ v_t &= -\left(uv_r + \frac{v}{r}v_\theta + \frac{vu}{r} + \frac{\Theta}{r}P_\theta\right), \\ P_t &= -\left(uP_r + \frac{v}{r}P_\theta + \gamma\left(u_r + \frac{v_\theta}{r} + k\right)\right), \\ s_t &= -\left(us_r + \frac{v}{r}s_\theta\right). \end{aligned} \tag{3}$$

3.1 Coordinate Transformation

To transform the governing equations from the physical domain (t, r, θ) to the computational domain (T, Z, Y), the following transformation is defined

$$\begin{aligned} T &= t, \\ Z &= \frac{r - b(\theta)}{c(t,\theta) - b(\theta)}, \\ Y &= \pi - \theta. \end{aligned} \tag{4}$$

In (4) the function $b(\theta)$ is the body radial coordinate and it is stationary, and $c(t, \theta)$ is the shock radial coordinate which is time dependent. The component of the bow shock velocity along a radial line is indicated by w.

For this transformation, the derivatives of an arbitrary function $f(t, r, \theta)$ are transformed to

$$\begin{aligned} \frac{\partial f}{\partial t} &= \frac{\partial f}{\partial T} + Z_t \frac{\partial f}{\partial Z}, \\ \frac{\partial f}{\partial r} &= Z_r \frac{\partial f}{\partial Z}, \\ \frac{\partial f}{\partial \theta} &= Z_\theta \frac{\partial f}{\partial Z} + Y_\theta \frac{\partial f}{\partial Y}. \end{aligned} \tag{5}$$

Applying the transformation to the governing equations

$$\begin{aligned} u_T &= -\left(U u_Z + V u_Y - \frac{v^2}{r} + \Theta Z_r P_r \right), \\ v_T &= -\left(U v_Z + V v_Y + \frac{vu}{r} + \frac{\Theta}{r} \left(Z_\theta P_Z + Y_\theta P_Y \right) \right), \\ P_T &= -\left(U P_Z + V P_Y + \gamma \left(Z_r u_Z + \frac{Z_\theta}{r} v_Z + \frac{Y_\theta}{r} v_Y + k \right) \right), \\ s_T &= -\left(U s_Z + V s_Y \right), \end{aligned} \tag{6}$$

where the contravariant velocity components are defined by

$$\begin{aligned} U &= Z_t + u Z_r + \frac{v}{r} Z_\theta, \\ V &= \frac{v}{r} Y_\theta, \end{aligned} \tag{7}$$

and the transformation metrics are given by

$$\begin{aligned} Z_t &= \frac{-Zw}{c-b}, \\ Z_r &= \frac{1}{c-b}, \\ Z_\theta &= \frac{Z(b_\theta - c_\theta) - b_\theta}{c-b}, \\ Y_\theta &= -1. \end{aligned} \tag{8}$$

The transformation from the physical plane to the computational plane is depicted in Figure 2. Specifically, the symmetry line is mapped onto the line $Y = 0$, while the bow shock is mapped onto the line $Z = 1$. Additionally, the outflow boundary is mapped onto the line $Y = \theta_{max}$, and the wall is mapped onto the line $Z = 0$.

4 Numerical Methods

Several possible explicit integration schemes exist. Among them is the Lax-Wendroff scheme, which was utilized by Moretti and Abbett when this problem was first solved [4]. Another option is the MacCormack predictor-corrector scheme, which became very popular later. Additionally, the lambda scheme can also be applied to this particular problem. Herein, MacCormack's scheme is used due to of its simplicity.

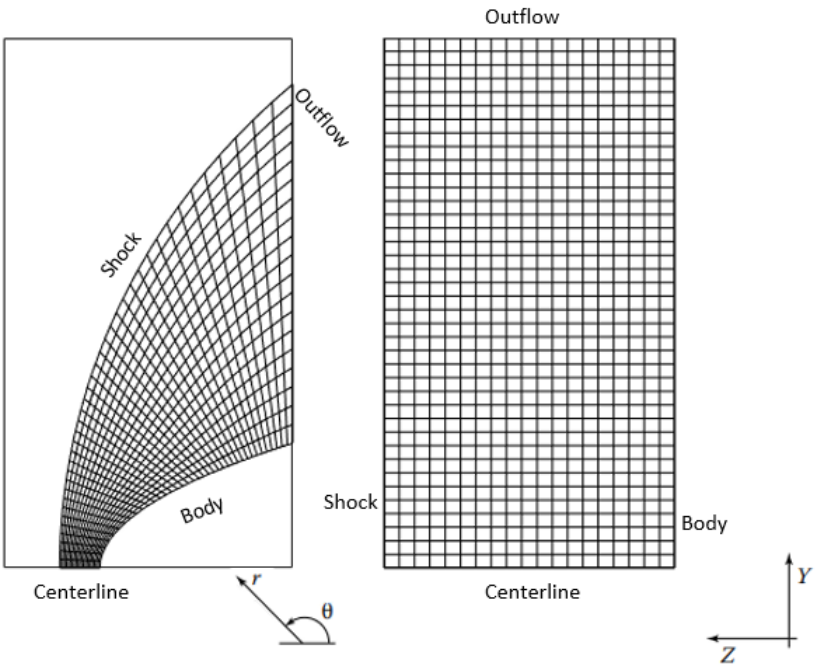

Fig. 2: The physical and computational grids

4.1 MacCormack's Scheme

The MacCormack scheme is applied to the above equations in two steps, starting with a predictor step and followed by a corrector step. These steps are applied to the solution variables u, v, s, P, w, c, η_r and η_θ.

First, a predicted value of an arbitrary variable, A, is calculated from the first two terms of a Taylor series expansion

$$\overline{A}_{i,j}^{t+\Delta t} = A_{i,j}^{t} + \left(\frac{\partial A}{\partial t}\right)_{i,j}^{t} \Delta t. \tag{9}$$

The calculation of $(\partial A/\partial t)^t$ involves the use of forward differences for the spatial derivatives.

Next, as a corrector step, the value of the time derivative is calculated by inserting the predicted values and using backward differences for the spatial derivatives

$$\left(\frac{\partial \overline{A}}{\partial t}\right)_{i,j}^{t+\Delta t}. \tag{10}$$

The final value of the variable is calculated by averaging the derivatives obtained from the previous predicted and corrected values

$$A_{i,j}^{t+\Delta t} = \frac{1}{2}\left[\left(\frac{\partial A}{\partial t}\right)_{i,j}^{t} + \left(\frac{\partial \overline{A}}{\partial t}\right)_{i,j}^{t+\Delta t}\right]. \tag{11}$$

After enough steps, i.e. for large times, a steady state will be approached, at which $A_{i,j}^{t+\Delta t} \approx A_{i,j}^{t}$.

Regarding the numerical accuracy of this method, which uses forward and backward differences on the predictor and corrector steps, the combination of the two steps results in a second-order accurate technique in space.

For a time-marching approach, the value of Δt must be addressed. The finite-difference method used here is an explicit method, and therefore Δt is subject to a stability criterion. The stability criterion is a version of the Courant–Friedrichs–Lewy (CFL) criterion, which governs the stability of explicit methods dealing with hyperbolic equations [5],

$$\Delta t < K \left[\min \left(\frac{\Delta r}{u + a}, \frac{\Delta \theta}{v + a} \right) \right], \tag{12}$$

where Δr and $\Delta \theta$ the are the distances between adjacent grid points in the r and θ directions, and a is the nondimensional local speed of sound, given by $a = \sqrt{\gamma \Theta}$.

The CFL criterion is derived based on an assumption of linearity. Therefore, for the nonlinear Euler equations a prefactor K is added, which is smaller than 1. In the current study a value of $K = 0.8$ is used.

4.2 Initial Conditions

The task of defining initial conditions for the blunt body problem can be challenging as it requires devising a suitable shape for the bow shock and assigning appropriate initial values to the flow variables within the shock layer. Salas [3] notes that the program is not very sensitive to the initial shape of the shock wave, and a parabolic profile was used to approximate the bow shock reasonably. However, our findings suggest the opposite, and we found that the program is indeed sensitive to the initial shock wave shape.

It is worth noting that Salas examined flows over relatively small portions of blunt bodies in his book, whereas in our work various types of bodies with different lengths are analyzed. Our research indicated that for small bodies, the program is not sensitive to the shape of the initial shock wave in accordance with the findings of Salas. However, for larger bodies, the initial shock wave shape has a significant influence on the program's performance.

Nevertheless, after conducting numerous runs of program for various body shapes and Mach numbers, we found that the parabolic profile was suboptimal. The best-suited initial shape, particularly for large bodies, where the program becomes highly sensitive to the initial shock, is the hyperbolic shock. This shape provides a good approximation away from the body, where the curved shock wave gradually becomes a Mach wave. Therefore, the following initial shape is used for the bow shock in the blunt body problem

$$c_0(x) = \sqrt{\frac{(x+\delta)^2 - d^2}{m}}, \tag{13}$$

where δ and m are two free parameters addressed below and d is an offset parameter which is taken from the body. For a convenience and simplicity, the initial body shape is provided in a standard Cartesian coordinate system (x, y) and then transformed into the working (r, θ) coordinate system.

The two free parameters are used to tune the bow shock shape. The parameter δ determines the shock detachment distance, while m controls the shock curvature. Both of these parameters require manual adjustment. It is worth noting that for small bodies, these parameters may have a single value that covers the entire range of Mach numbers. However, for larger bodies, these parameters need to be readjusted for each variation in order to get a solution.

By approximating the bow shock shape using equation (13), the flow field on the high pressure side of the shock can be determined by applying the Rankine-Hugoniot conditions. The stagnation conditions at the nose of the blunt body are precisely known, as the streamline that touches the body coincides with the streamline on the symmetry line. With the modified Newtonian pressure distribution and no penetration condition, the flow field on the body can be defined using these known stagnation conditions. The remaining part of the shock layer is initialized by linearly interpolating the flow variables between the bow shock and the body along lines of constant Y.

4.3 Wall Computation

At the wall, a fixed frame of reference is taken (η, τ) whose axes are normal and tangent to the wall at the point of interest. Let $\hat{\eta}$ be the unit normal pointing to the wall, such that

$$\begin{aligned} \hat{\eta} &= \eta_r \hat{r} + \eta_\theta \hat{\theta}, \\ \hat{\tau} &= \eta_\theta \hat{r} - \eta_r \hat{\theta}, \end{aligned} \tag{14}$$

where

$$\begin{aligned} \eta_r &= \frac{-1}{\sqrt{1 + \left(\frac{c_\theta}{c}\right)^2}}, \\ \eta_\theta &= \frac{\frac{c_\theta}{c}}{\sqrt{1 + \left(\frac{c_\theta}{c}\right)^2}}, \end{aligned} \tag{15}$$

and c_θ is the derivative of the shock shape, c, in the θ direction.

Let $\tilde{u}, \tilde{v}$ be the velocity components in the η, τ directions, respectively. The boundary condition at the wall is $\tilde{u} = 0$, which implies that $\tilde{u_T} = 0$. Combining the two momentum equations in (6) into a momentum equation in the tangential direction at the wall we are left with

$$\begin{aligned} \tilde{v}_T &= -\left(V\tilde{v}_Y + \frac{\Theta}{r} Y_\theta P_Y \eta_r \right), \\ P_T &= -\left(V P_Y + \gamma \left(\frac{Z_r \tilde{u}_Z}{\eta_r} + \frac{Y_\theta v_Y}{r} + k \right) \right), \\ s_T &= -V s_Y, \end{aligned} \tag{16}$$

and

$$\begin{aligned} v_T &= -\tilde{v}_T \eta_r, \\ u_T &= \tilde{v}_T \eta_\theta. \end{aligned} \tag{17}$$

Equations (16) and (17) are integrated using MacCormack's scheme, which is employed for the rest of the field.

4.4 Shock Computation

The Rankine-Hugoniot equations are used to determine all the flow variables at the shock boundary, but for the calculation of the shock velocity at the next step its derivative, i.e. the shock acceleration, w_T, is required. Fortunately, by utilizing the method of characteristics, it is possible to obtain an equation for w_T. On the characteristic cones λ^+, λ^- information is propagated, and a combination of flow variables remains constant. This information is encapsulated in the following Riemann invariants

$$\begin{aligned} R &= \frac{2a}{\gamma - 1} + u \quad on\ \lambda^+, \\ Q &= \frac{2a}{\gamma - 1} - u \quad on\ \lambda^-. \end{aligned} \tag{18}$$

The information carried on the high-pressure side of the shock is in the λ^- direction. Then the appropriate Riemann invariant to use is

$$Q_2 = \frac{2a_2}{\gamma - 1} - \tilde{u}_2, \tag{19}$$

where the subscript 2 denotes values on the high-pressure side of the shock. Here, $\tilde{u} = (u\hat{r} + v\hat{\theta}) \cdot \hat{\eta}$, and the shock acceleration can be determined by relating Q_2 to $M_{1,rel}$ using the Rankine-Hugoniot jump, where $M_{1,rel}$ denotes the relative Mach number, signifying the Mach number utilized in Rankine-Hugoniot relations. It differs from the freestream Mach number since the shock wave is moving.

The Rankine-Hugoniot relations in terms of the relative Mach number are

$$\begin{aligned}
\frac{p_2}{p_1} &= \frac{2\gamma M_{1,rel}^2 - (\gamma-1)}{\gamma+1}, \\
\frac{\rho_2}{\rho_1} &= \frac{(\gamma+1)M_{1,rel}^2}{(\gamma-1)M_{1,rel}^2+2}, \\
M_{2,rel}^2 &= \frac{(\gamma-1)M_{1,rel}^2+2}{2\gamma M_{1,rel}^2-(\gamma-1)},
\end{aligned} \tag{20}$$

where

$$M_{i,rel} = \frac{\tilde{u}_i - \tilde{w}}{a_i}, \qquad i = 1, 2. \tag{21}$$

The velocity of the shock along the normal direction is denoted by $\tilde{w}$, whereas in the code the shock moves in the radial direction with velocity w. Therefore, the suitable conversion between the two is

$$\tilde{w} = w\eta_r. \tag{22}$$

The speed of sound on the high pressure side, a_2, is obtained from the first and second equations in (20), whereas $\tilde{u}_2$ is provided by the third equation.

$$\begin{aligned}
a_2 &= \sqrt{\frac{\gamma p_2}{\rho_2}}, \\
\tilde{u}_2 &= \sqrt{\frac{\gamma p_2}{\rho_2}\left(\frac{(\gamma-1)M_{1,rel}^2+2}{2\gamma M_{1,rel}^2-(\gamma-1)}\right)} + \tilde{u}_1 - a_1 M_{1,rel}.
\end{aligned} \tag{23}$$

The above equation is formulated using the variables denoted by the subscript 1, with the aim of establishing a connection between Q_2 and the pre-shock variables. Ultimately, this connection between Q_2 and $M_{1,rel}$ is established by substituting the first and second expressions from (23) into (19) and simplifying.

$$\begin{aligned}
\frac{\gamma+1}{2a_1}(Q_2 - \tilde{u}_1) &= g(M_{1,rel}), \\
g(M_{1,rel}) &= \sqrt{\frac{\left(2\gamma M_{1,rel}^2-(\gamma-1)\right)\left((\gamma-1)M_{1,rel}^2+2\right)}{(\gamma-1)^2 M_{1,rel}^2}} - \frac{1+\gamma M_{1,rel}^2}{M_{1,rel}}.
\end{aligned} \tag{24}$$

The equation for the shock acceleration can be obtained by differentiating equation (24) with respect to T,

$$g_T = \frac{\gamma+1}{2a_1}\left(Q_{2,T} - \widetilde{u}_{1,T}\right), \tag{25}$$

The function g is differentiated by the chain rule with $g' = \partial g/\partial M_{1,rel}$

$$g_T = g' \cdot M_{1,rel,T} \;= g' \cdot \frac{\tilde{u}_{1,T} - w_T\eta_r - w\eta_{r,T}}{a_1} = \frac{\gamma+1}{2a_1}\left(Q_{2,T} - \tilde{u}_{1,T}\right), \tag{26}$$

where

$$\eta_{r,T} = \frac{-\left(\, w_Y + w\frac{c_\theta}{c}\right)}{\sqrt{1+\left(\frac{c_\theta}{c}\right)^{\frac{3}{2}}}},$$
$$\eta_{\theta,T} = \frac{-\left(\, w_Y + w\frac{c_\theta}{c}\right)\frac{c_\theta}{c}}{\sqrt{1+\left(\frac{c_\theta}{c}\right)^{\frac{3}{2}}}}. \tag{27}$$

It should be noted that the computation of $\eta_{r,T}$ and $\eta_{\theta,T}$ involves the addition of two small quantities, w_Y and wc_θ/c, which become zero in the steady state. However, this computation may suffer from odd-even oscillations that can be mitigated by employing a weighted average of $\eta_{r,T}$ and $\eta_{\theta,T}$.

Finally, the shock acceleration is given by

$$w_T = \frac{1}{\eta_r}\left(\left(1+\frac{\gamma+1}{2g'}\right)\tilde{u}_{1,T} - \frac{\gamma+1}{2g'}Q_{2,T} - w\eta_{r,T}\right). \tag{28}$$

In order to evaluate $Q_{2,T}$, it is expressed in terms of primitive variables

$$a_{2,T} = \frac{\gamma-1}{2\gamma}a_1\left(P_T + \frac{s_T}{\gamma-1}\right), \tag{29}$$
$$\tilde{u}_{2,T} = u_T\eta_r + u\eta_{r,T} + v_T\eta_\theta + v\eta_{\theta,T},$$
$$Q_{2,T} = \frac{a_1\left((\gamma-1)P_T + s_T\right)}{\gamma(\gamma-1)} - \tilde{u}_{2,T} \tag{30}$$

The internal predictor-corrector algorithm can be used to obtain the time derivatives of the primitive variables (P_T, s_T, u_T, v_T), which can then be used to evaluate $Q_{2,T}$.

The flow chart of the code is given in appendix B.

5 Results

5.1 Blunt Body Program

The shape and position of the shock wave for different blunt bodies and freestream Mach numbers (3, 5, 7, and 12) is shown in figures 3, 4, 5 and 6, based on the analysis presented in our previous report [1]. The calculations were performed using a 40x80 grid points for a calorically perfect gas with a specific heat ratio of 1.4. Similarly to the initial shock shape, the blunt body shapes are given in the standard Cartesian coordinate system (x, y). The offset is defined as the distance between the tip of the body and the origin.

Body	Equation	Offset
Parabolic	$y_b = \sqrt{2x+4}$	4
Cubic	$y_b = \sqrt[3]{2x+4}$	4
Hyperbolic	$y_b = \sqrt{\frac{(x+4)^2-4}{2}}$	4
Elliptic	$y_b = \sqrt{\frac{4-x^2}{2}}$	3

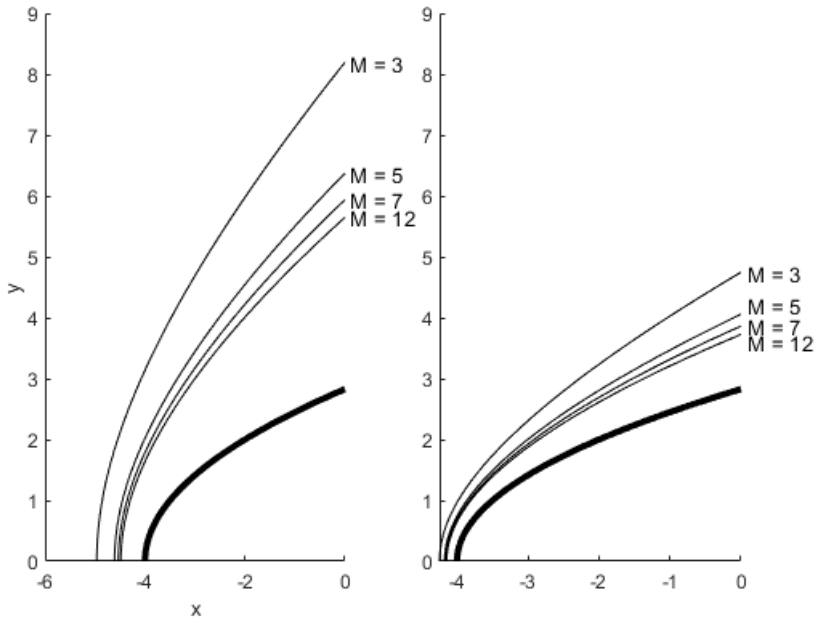

Fig. 3: Parabolic body; (left) plane flow (right) axisymmetric flow

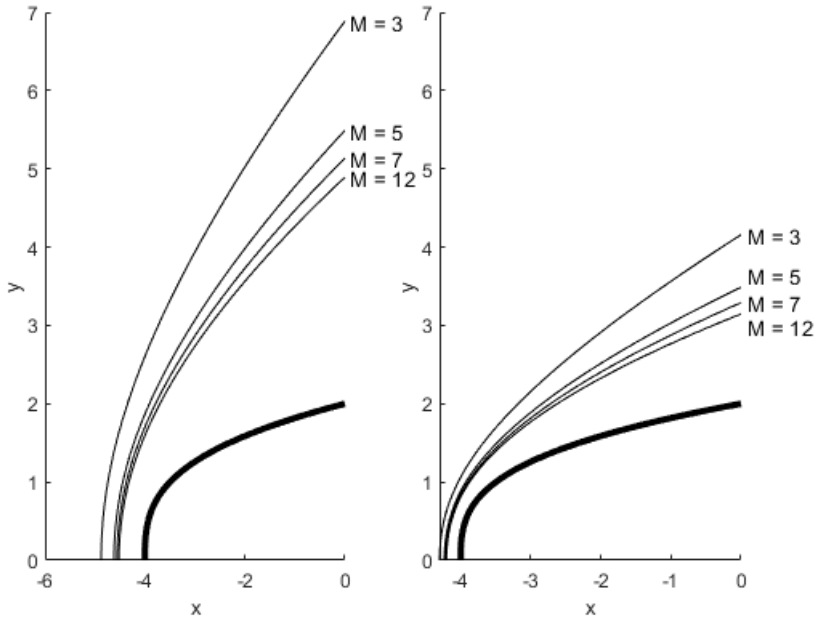

Fig. 4: Cubic body; (left) plane flow (right) axisymmetric flow

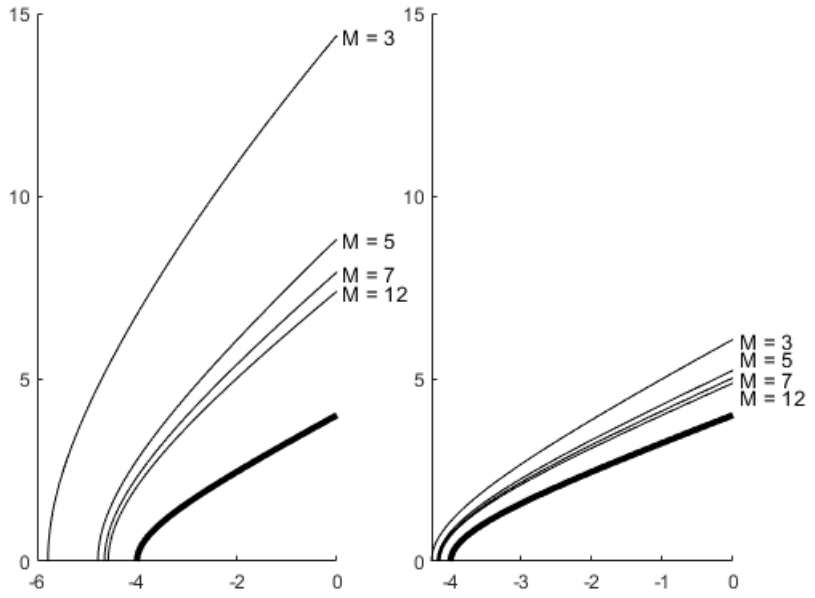

Fig. 5: Hyperbolic body; (left) plane flow (right) axisymmetric flow

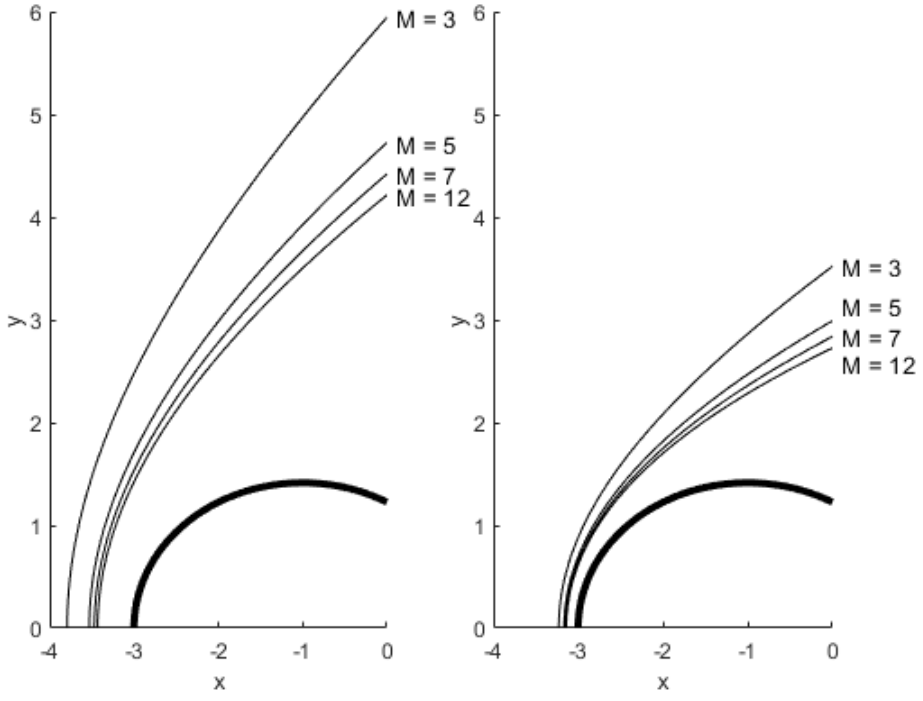

Fig. 6: Elliptic body; (left) plane flow (right) axisymmetric flow

Figures 3, 4, 5 and 6 demonstrate the effectiveness of the blunt body program in producing accurate and efficient results for a wide range of Mach numbers and various types of blunt bodies in both plane and axisymmetric flows. The figures depict the bow shock shape and how it changes in response to the geometry of the blunt body and the Mach number of the freestream flow. The comprehensive visualization offered by the figures provides a valuable tool for analyzing the physical behavior of blunt body flows. For a more detailed analysis of the physical phenomena involved in the blunt body problem, readers are referred to our previous work (Ref. [1]).

5.2 Grid Convergence

Figures 7 and 8 investigate the spatial convergence of the solution by plotting two parameters, namely the shock detachment distance δ and stagnation pressure p_0, against a grid parameter m_r, which represents the number of points in the radial direction, while the number of points in the theta direction is always double. The computation was performed for a plane flow over a parabolic body at a freestream Mach number of 4. It is evident that accurate results can be obtained with a relatively small number of points.

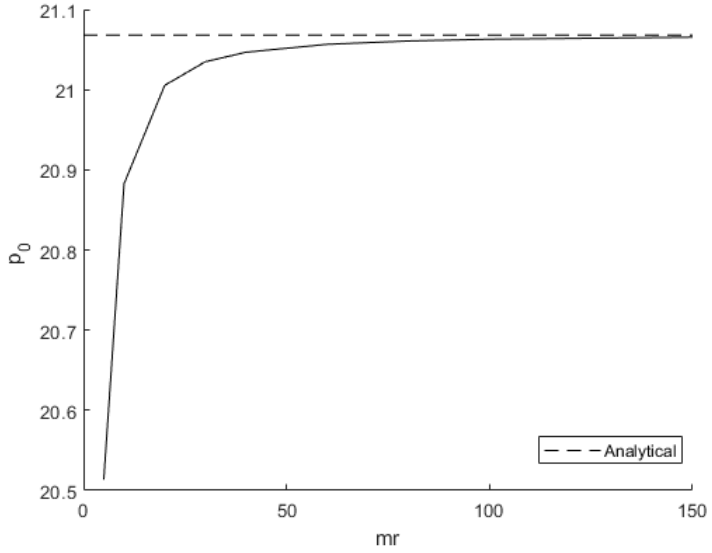

Fig. 7: Normalized stagnation pressure versus the number of points in the radial direction ($m_\theta = 2m_r$)

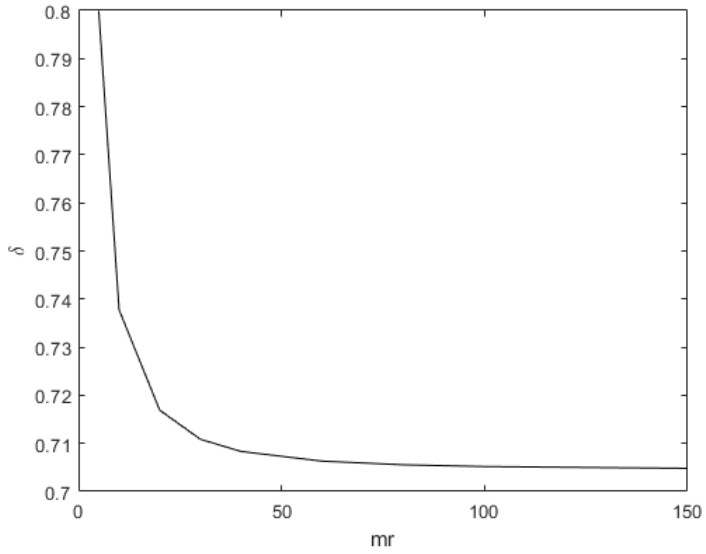

Fig. 8: Shock detachment distance versus the number of points in the radial direction ($m_\theta = 2m_r$)

6 Summary

The focus of this study is on improving the accuracy and efficiency of simulations for the supersonic blunt-body problem. Our previous work has faced challenges such as oscillations near the outflow boundary and limited flow field in the axisymmetric scenario. In this study, a new approach is proposed to overcome these issues by implementing boundary conditions that include utilization of Riemann variables to obtain the shock acceleration. Additionally, a new coordinate system is introduced which enhances the mesh at the outflow, enabling us to solve for a variety of blunt body shapes at different speeds and flow conditions using a relatively coarse computational mesh. The significance of our program lies in its ability to provide an accurate base flow for the study of the stability properties of the blunt body flow, which is a critical aspect for future research.

Appendices

A Nondimensionalization

The pressure, density and temperature are nondimensionalized by their freestream values p_∞, ρ_∞, Θ_∞. The velocity is normalized by $\sqrt{p_\infty/\rho_\infty}$, which gives the freestream speed of sound $a_\infty = \sqrt{\gamma}$ and freestream velocity $u_\infty = M_\infty\sqrt{\gamma}$.

The equation of state becomes

$$p = \rho\Theta. \tag{31}$$

The entropy is normalized by c_v, therefore

$$s = \gamma \ln\Theta - (\gamma - 1)\ln p, \tag{32}$$

and the Crocco theorem in dimensionless quantities is

$$\boldsymbol{\omega} \times \boldsymbol{u} = \frac{\Theta\nabla s}{\gamma - 1}. \tag{33}$$

B Flowchart of the code

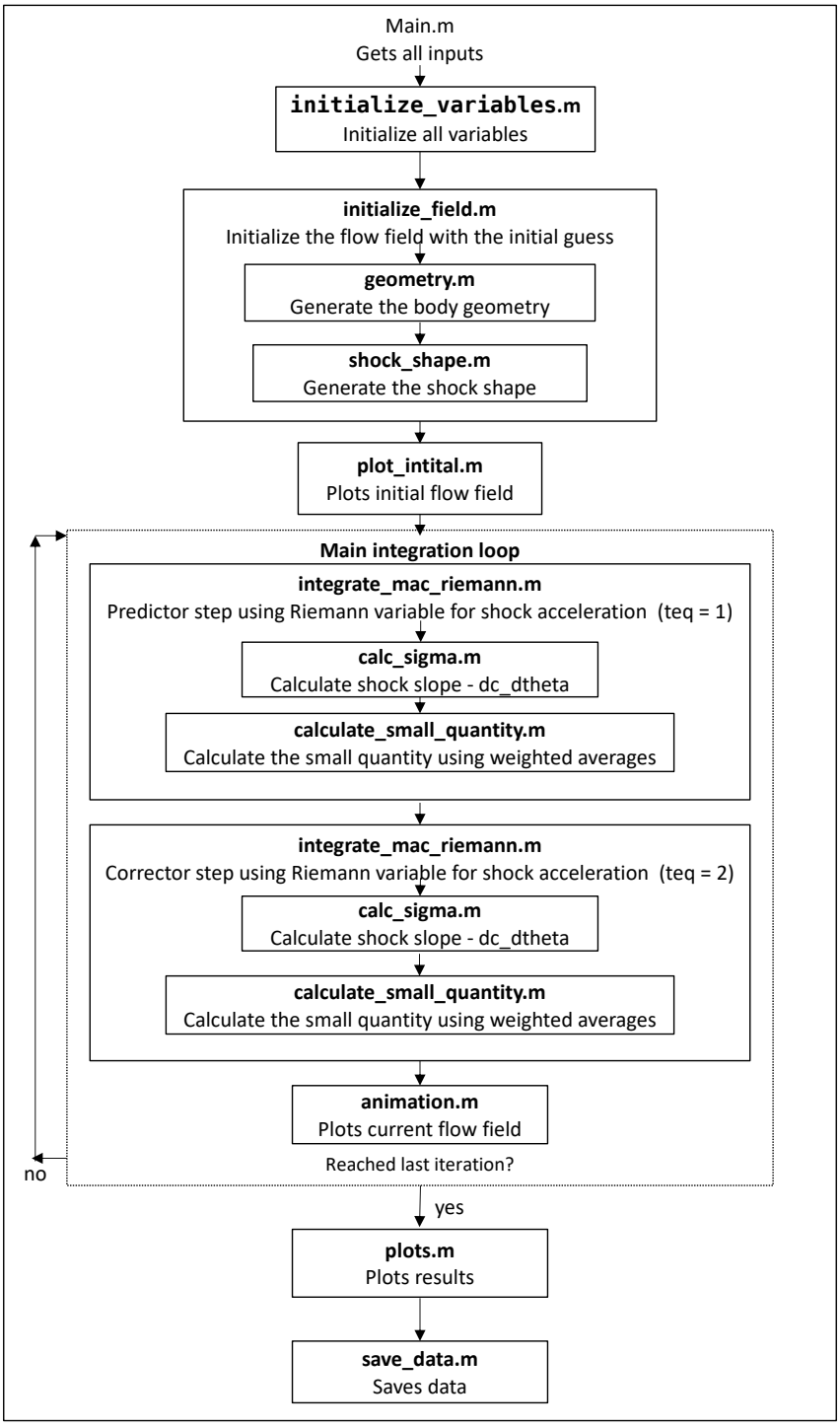

Fig. 9: Flowchart of the code

References

[1] I. Milman and M. Karp, *An Investigation of the Supersonic Blunt-Body Problem.* Research Project, 2022.

[2] J. D. Anderson, *Hypersonic and high temperature gas dynamics.* AIAA, 2000.

[3] M. D. Salas, *A shock-fitting primer.* CRC Press, 2009.

[4] G. Moretti and M. Abbett, "A time-dependent computational method for blunt body flows," *AIAA J.*, vol. 4, no. 12, pp. 2136–2141, 1966.

[5] R. Courant, K. Friedrichs, and H. Lewy, "Über die partiellen differenzengleichungen der mathematischen physik," *Mathematische annalen*, vol. 100, no. 1, pp. 32–74, 1928.